Hindawi Publishing Corporation
International Journal of Antennas and Propagation
Volume 2014, Article ID 875345, 8 pages
http://dx.doi.org/10.1155/2014/875345

Research Article

Measurement-Based Delay and Doppler Characterizations for High-Speed Railway Hilly Scenario

Yan Zhang,[1] Zunwen He,[1] Wancheng Zhang,[1] Limin Xiao,[2] and Shidong Zhou[2]

[1] *School of Information and Electronics, Beijing Institute of Technology, Beijing 100081, China*
[2] *Tsinghua National Laboratory for Information Science and Technology, Department of Electronic Engineering, Tsinghua University, Beijing 100084, China*

Correspondence should be addressed to Yan Zhang; zhangy931@gmail.com

Received 5 December 2013; Revised 28 March 2014; Accepted 28 March 2014; Published 15 April 2014

Academic Editor: Jianhua Zhang

This paper presents results for delay and Doppler spread characterization in high-speed railway (HSR) hilly scenario. To investigate the propagation characteristics in this specific terrain, a measurement campaign is conducted along the "Guangzhou-Shenzhen" HSR in China. A wideband channel sounder with 40 MHz bandwidth is used to collect raw data at 2.4 GHz band. The delay spread and Doppler frequency features are analyzed based on measured data. It is found that there are abundant multipath components (MPCs) in this scenario. We present the relationship between the delay spreads and the transceiver distances. The measured route can be divided into four areas with different delay and Doppler characteristics. Finally, a tapped delay line (TDL) model is proposed to parameterize the channel responses in the HSR hilly environment, which is supposed to provide criterions for evaluations of the radio interface and development of wireless communication system.

1. Introduction

In recent years, high-speed railway (HSR) has noticeable development in many countries. In China, more and more HSRs have been built and operated [1]. At the same time, there is an increasing demand for using cell phones, laptops, and Tablet PCs conveniently on the HSR trains. To realize efficient and reliable wireless access on HSR, one fundamental work is to investigate the propagation characteristics in typical environments. Compared with conventional urban or suburban scenarios, the environment along HSR usually has its own features, for example, in most cases the railway is built on the viaduct far away from the urban area. In addition, high-speed mobility can bring fast time variation to channel responses, which affects the signal processing [2]. Consequently, it is indispensable to build channel model for HSR propagation environment, which can provide references for the wireless system design, simulation, and verification.

The HSR propagation environment can be classified into different scenarios, including viaduct, hilly terrain, tunnel, cutting, and station [2, 3]. Recently, some measurement-based studies have been carried out in viaduct [4–7], tunnel [8–11], and cutting [12, 13] scenarios. Field strength results at 320 MHz band for different scenarios can be found in [14]. In [4], a position-based model is established under a viaduct scenario. For rural moving network, a so-called D2a model is presented in WINNER II project [15]. In 3GPP TS36.104 [16], the HSR propagation conditions are defined for open space and tunnel scenarios. The in-carriage channel parameters are also measured and analyzed in [17, 18].

However, there is still a lack of research about the HSR hilly scenario. For example, the hilly terrain occupies about 2/3 area of China, and the newly-built HSRs in south and west China, such as the Guangzhou-Shenzhen and Chengdu-Guiyang passenger dedicated lines, run through vast area in hilly terrain. Compared with other scenarios, the HSR hilly propagation environment has its own characteristics, for example, numerous reflectors along the railway may lead to different multipath propagation characteristics. In the HSR wireless system design process, we need to consider all scenarios with different delay and Doppler spreads to ensure

the system can work in any case; thus it is important to conduct the channel measurement and modeling work for HSR hilly scenario.

In our previous work [19], the fading characteristics in HSR hilly scenario are analyzed from the measured channel data. The path loss, shadow, and small scale fading are parameterized with position-based models, which can serve as a reference for HSR communication coverage planning. In that study, it is proved that not only the line-of-sight (LoS) path but also the diffused paths exist in hilly environment. In this paper, we mainly focus on the multipath effects, especially the delay dispersion and Doppler shift property in HSR hilly scenario, which are also of great significance to the future communication system design.

In this paper, the relationship between channel parameters and the transmitter-receiver (T-R) distance is discussed. A high-resolution estimation algorithm, Subspace Alternating Generalized Expectation- (SAGE-) maximization algorithm, is utilized to estimate the parameters in different domains. The resolvable number of multipath components (MPCs) is extracted from measured data. Then the maximum excess delay and root mean square (RMS) delay spread are analyzed for different areas. The Doppler spectrums at different receiver positions are also shown. A tapped delay line (TDL) model is proposed to describe the wideband channel responses in HSR hilly scenario.

The main contributions of this paper are listed as follows. The existence of MPCs is proved in HSR hilly scenario and these MPCs can lead to time and frequency dispersions. We illustrate the relationship between the transceiver distance and channel parameters including the resolvable MPC number, the RMS delay spread and the maximum excess delay. The propagation route can be divided into four partitions with different channel characteristics. The Doppler spectrums at different partitions are also shown and summarized. Based on the above analyses, we derive a TDL channel model for the HSR hilly scenario as a promotion for wireless system evaluation.

The remainder of this paper is organized as follows. The measurement setups and data processing methods are introduced in Section 2. In Section 3, we parameterize the delay spread and discuss its relationship with receiver position. In Section 4, the Doppler shift feature is depicted. A TDL model for HSR hilly scenario is proposed in Section 5. Finally, our conclusions are presented in Section 6.

2. Channel Measurements

2.1. Measurement Setups. The measurement campaign was finished in Guangzhou-Shenzhen passenger dedicated line with 104 km length and 350 kph designed speed. The major scenarios along this HSR contained hilly, viaduct, and tunnel terrain types, while in this study the hilly scenario would be mainly considered.

The selected area is 63 km from Guangzhou and 41 km from Shenzhen, whose aerial view is shown in Figure 1. The selected surrounding environment is a typical hilly terrain and its radius is about 1300 m. The white line illustrates the measured route while the yellow marker indicates the base station (BS). Undulating hills around the railway are almost below 200 m. On the south side of the railway, there are two regions with buildings about 800 m and 2200 m far from the BS, respectively.

Figure 1: Aerial map of measured hilly area. The white line indicates the railway and the marker indicates the base station.

In this measured hilly scenario, rich reflections and scatterings can be expected, which will make arriving signal suffer from multipath effect. The LoS path is still strong because there are no significant obstacles between BS and train, while different MPCs can also be received. This multipath effect can bring the dispersions in both delay and Doppler frequency domains.

Tsinghua University (THU) channel sounder [20] was used to collect raw measured data. During the measurement campaigns, it worked at 2.4 GHz central frequency with 40 MHz bandwidth. The major configurations of this measurement campaign were shown in Table 1. The transmitting power is 20 dBm and the dynamic range of the receiver is from −103 dBm to −61 dBm.

A single-input single-output system was constructed and the transmitting antenna was fixed on a BS tower with 30 m height. The track distance from BS to railway was 10 m. The transmitter at the BS included the signal generator, the rubidium clock reference, and the power amplifier. The test signal was feed to the transmitting antenna by a low insertion loss cable, and the total radiated signal power was 20 dBm. The transmitting antenna was a directional antenna with 17 dBi gain pointing at the train forward direction.

The receiver was mounted in the train carriage, which also employed a rubidium clock to eliminate the synchronization offsets between receiver and transmitter. The omnidirectional receiving antenna with 7 dBi gain was fixed on the window inside the carriage. Different from the high speed and mobile cell (Himocell) coverage mode [4], the direct coverage scheme of HSR was considered in our work; that is, the receiver directly established a link to the BS without a gateway [21].

The measurement was carried out while the HSR was in the trial operation stage. There were no passengers or any other moving objects in the carriage during our measurement procedure, so the in-carriage propagation environment can be considered as quasi-stationary. GPS navigation was used to record the mobile speed and positions and the speed of train was 295 kph during the measurement campaign according to it.

Table 1: Configurations of the measurement campaign.

Parameter	Setting
Central frequency	2.4 GHz
Bandwidth	40 MHz
Transmitting signal length	12.8 μs
Transmitting power	20 dBm
Transmitting antenna height	30 m
Receiving antenna height	1.2 m
Track distance from BS to railway	10 m
Moving speed	295 kph

2.2. Data Processing. The test signal is a linear frequency modulated (LFM) sequence with autocorrelation feature. The sequence length is 12.8 μs which is corresponding to the maximum excess delay range. The receiver collects and stores the real-time signal as well as the GPS information, which is processed offline. The received sequence is correlated with the local copy of the transmitting LFM signal to acquire the channel impulse responses. In addition, the data is calibrated considering the frequency response and group delay of RF units.

To extract the MPC information from the channel impulse responses, we utilized a high-resolution estimation method, SAGE algorithm [22], which is a low-complexity approximation of the maximum likelihood (ML) estimation. And it is able to distinguish the parameters of MPCs with low computational complexity. To extract the multipath components, we select 20 snapshots in a very small region for SAGE processing at different train positions. Because the moving distance is smaller than the coherence distance, the channel response almost keeps invariant in this small region. So the multipath components can be viewed as time-stationary. Then the received signal can be assumed as a superposition of a finite number of specular waves:

$$r(t) = \sum_{l=1}^{L} \alpha_l \exp\{-j2\pi\nu_l t\}\, s(t-\tau_l). \quad (1)$$

Each wave is characterized by its relative delay τ_l, Doppler frequency ν_l, and complex amplitude α_l, respectively. These parameters can be estimated simultaneously by using SAGE algorithm. L is the total number of MPCs which needs to be predefined. In our estimation process, $L = 40$, which is to ensure that most received energy is included. In most cases, the predefined MPC number will be larger than the realistic MPC number. That means that there may be some artificial MPCs which are actually the noises in these estimated MPCs. So we choose a noise threshold which is 3 dB higher than the noise floor. The MPCs under this noise threshold will be viewed as noise and discarded, in order to avoid erroneous results due to spurious components. Then we can calculate the time-varying delay and Doppler spreads.

During the measurement campaign, the train moves from west to east and the start point is about 160 m west from the BS. In the following analysis, the zero point is set at the intersection point of the railway track and the perpendicular line from the BS. Then the relationship between the transceiver distance and the channel parameters will be discussed in the following sections.

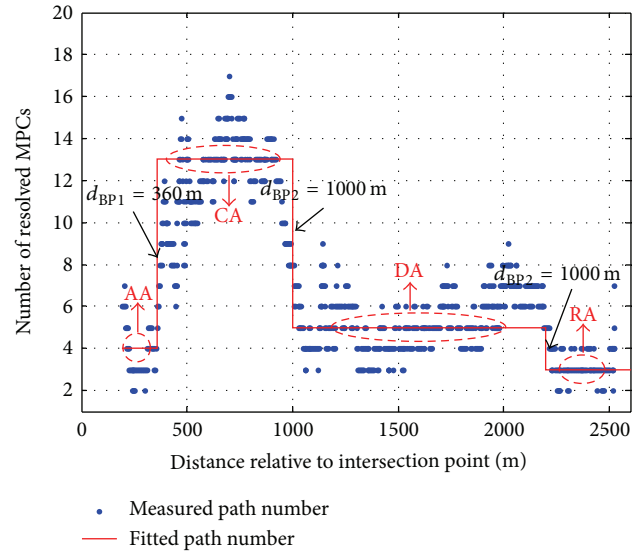

Figure 2: The resolvable MPC number in HSR hilly scenario.

3. Delay Dispersion Characteristics

3.1. Resolvable MPC Number. In 3GPP TS36.104 [16], only LoS path is taken into account in HSR open space and tunnel scenarios. However, according to previous measurement-based results [4, 19], it is revealed that MPCs also exist in typical HSR environment. These MPCs with different delays will bring the selective frequency fading to channel responses, which is important for future wideband communication systems, for example, the cyclic prefix (CP) design in the OFDM systems.

In hilly scenario, both the transmitter and receiver have many reflectors in their close vicinities. More MPCs can be expected because of complicated surrounding environment. In addition, there can also be long echoes from remote reflectors. In Figure 2, the resolvable MPC numbers are shown corresponding to different receiver positions. It can be seen that the number of MPCs is dependent on the train position and its changing process can be divided into several partitions. Three breakpoints (d_{BP1}, d_{BP2}, and d_{BP3}) can be empirically selected at 360 m, 1000 m, and 2200 m from the intersection point. Similar to the terminology in [4], we define these four partitions as adjacent area (AA), close area (CA), distant area (DA), and remote area (RA).

In Figure 2, the MPC number is relatively small when the train is near the BS. The LoS path between BS and train is dominant and the contribution from reflectors is small.

With the increase of T-R distance, the reflectors start to play an important role. In the CA, that is, $d_{BP1} < d < d_{BP2}$, more than ten reflected waves can be observed. Distributed hills together with buildings near the railway reflect the transmitting signal and produce several resolvable MPCs in this area.

When the train is apart from the BS, the propagation distances increase which lead to large attenuations to both LoS path and the reflected MPCs, and the resolvable MPC number decreases accordingly. In addition, there is an obvious decrease of MPC number near the break point d_{BP2}. In Figure 1, we can see that there are hills quite near the railway in this area, which block some MPCs from the reflectors to the train. Only about five waves can be received in this area.

In the remote area, that is, the distance is beyond d_{BP3}, very few MPCs including the LoS path can be resolved. Most of echoes are below the noise threshold and vanish in the power delay profile.

Compared with the HSR viaduct scenario [4], the hilly terrain has a larger number of resolvable MPCs, especially in CA. As mentioned above, this is caused by the complicated surrounding environment.

3.2. Delay Spread Analysis. Delay spread presents the delay dispersion brought by MPCs to wireless channel responses, which leads to selective fading in frequency domain.

The relative parameters are the maximum excess delay and RMS delay spread. The maximum excess delay is the time delay difference between the last arriving signal and the first arriving signal. It is defined as [23]

$$\tau_{\max} = \tau_x - \tau_1, \tag{2}$$

where τ_1 is the first arriving wave delay and τ_x is the maximum delay of the last signal whose power is above the noise floor. The RMS delay spread is another commonly used parameter to describe the dispersion. It is the square root of the second central moment of the power delay profile and can be defined as [23]

$$\sigma_\tau = \sqrt{\frac{\sum_l P(\tau_l)(\tau_l - \overline{\tau})^2}{\sum_l P(\tau_l)}}, \tag{3}$$

where $P(\tau_l)$ is the power of the lth path ($l = 1, \ldots, L$) and τ_l is the propagation delay of the lth path. $\overline{\tau}$ is the first moment of the instantaneous power delay profile and can be computed as

$$\overline{\tau} = \frac{\sum_l P(\tau_l)\tau_l}{\sum_l P(\tau_l)}. \tag{4}$$

Figure 3 shows the RMS delay spread as a function of transceiver distance. It is illustrated that the RMS delay spread values can also be divided into partitions by these break points. The LoS path plays the dominant role when the train is near BS. As the T-R distance increases, the value of RMS delay spread increases in general. There is an acute drop at the breakpoint d_{BP2}, where there are hills blocking many reflected MPCs.

Beyond d_{BP2}, the energy of LoS path is relatively low and the reflected paths become important for delay spread values. In this area there are numerous buildings, factories, and warehouses near the railway besides the rolling hills, as shown in Figure 1. The RMS delay spread varies in a wide range which may be caused by the death-and-birth processes

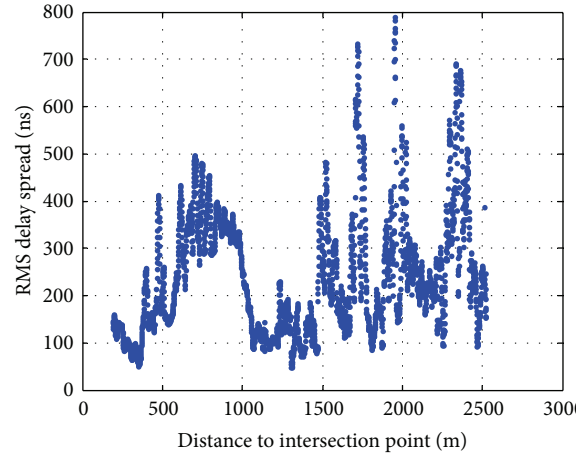

Figure 3: RMS delay spread in HSR hilly terrain.

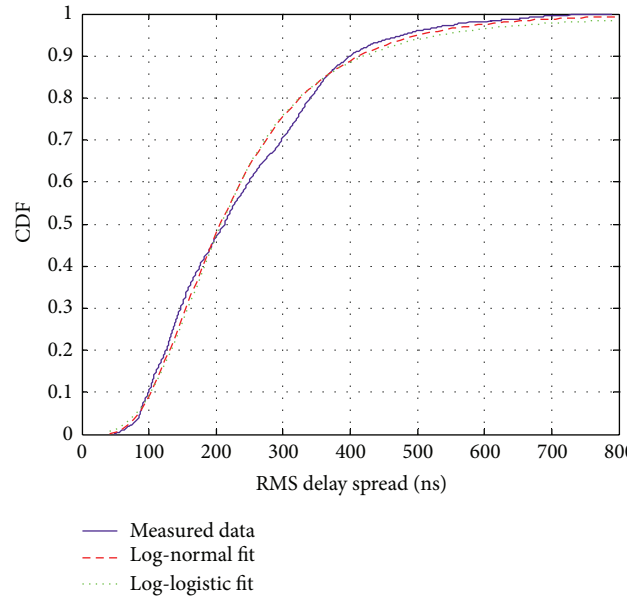

Figure 4: CDF of RMS delay spread values in HSR hilly terrain.

of some strong MPCs. For example, in Figure 3 there are abrupt rises near the 1700 m, 1900 m, and 2300 m from the intersection point. The delay spread jumps from low value up to about 700 nanoseconds at these positions. This may be caused by a strong reflection from a nearby "radio mast" [24] which is quite common in this scenario. The probability of this kind of these reflections (or abrupt rises of the RMS delay spread) is related to the density and distribution of buildings and is not possible to be estimated in our measurement campaign.

In Figure 4, the cumulative density function (CDF) of RMS delay spreads in the HSR hilly scenario is shown. RMS delay spread values are given for all the positions at the measured route. Here x-axis is the delay spread (in *ns*) and y-axis is the CDF. Fitting the measured RMS delay spread with different theoretic distributions is also shown in Figure 4. The red dash and the green dot line are the log-normal and

Table 2: The delay spread statistics in HSR hilly terrain.

	RMS delay spread (ns)	Max excess delay (ns)
10%	99.1	580
50%	212.1	1390
90%	400.8	2260
Mean	237.9	1541

log-logistic distributions, respectively. It can be seen that the log-normal distribution performs a little better. Then we can use log-normal distribution to describe the variation of delay spreads [25]:

$$\sigma_\tau = 10^{\varepsilon_\tau X + \mu_\tau}. \quad (5)$$

Here X is a standard Gaussian variable with zero mean and unit variance, while μ_τ and ε_τ are the mean value and standard deviation of $\log \sigma_\tau$. $\mu_\tau = -6.69$, $\varepsilon_\tau = 0.24$ according to our measured data in HSR hilly scenario.

The 10%, 50%, and 90% values for the CDF of the RMS delay spread values are listed in Table 2. Here the 90th percentile is the value for which 90% of the data points are smaller. At most receiver positions, the RMS delay spreads are less than 400 ns. It means that the major power of the MPCs is relatively concentrated although the path number is large. In this scenario, the railway is surrounded by hills and the distances from the railway to hills are limited. In other words, the reflections mostly happen in a "confined" area, which will also be verified in the maximum excess delay analysis.

Figure 5 illustrates the maximum excess delay values with different T-R distances. In most areas, the maximum excess delay is over 500 ns. In Figure 5, we can see that some maximum excess delay values can form discontinuous lines. Each line represents a reflector in the forward direction of train. When the train is moving to the reflector from far and near, the maximum excess delay determined by this reflected wave decreases because the T-R distance is shortened. Figure 5 shows that new MPC with larger excess delay will emerge when the propagation distance of this old reflected wave becomes weak.

The distribution of the maximum excess delay values is also analysed according to the measured data. The probability density function (PDF) and CDF of the maximum excess delays are shown in Figure 6, and the 10%, 50%, and 90% values for the CDF are given in Table 2. As illustrated in Table 2, the MPCs mostly arrive within 2260 ns after the arriving of the first arriving component. Similarly, the maximum excess delay values are not very large, which means the travelling distances of all MPCs are restricted. This phenomenon may also be due to the confined propagation region in HSR hilly scenario.

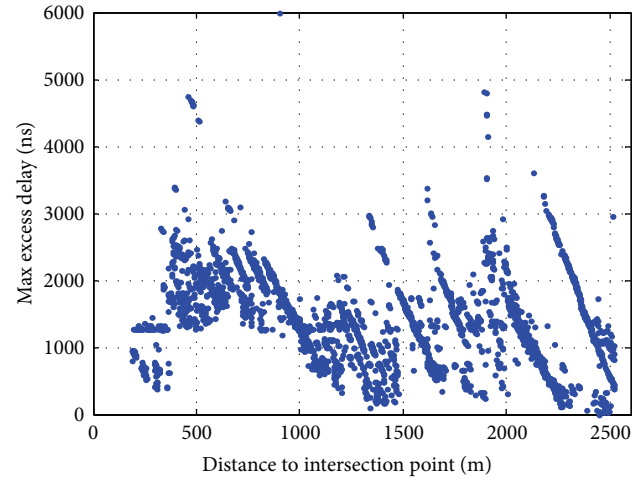

Figure 5: Maximum excess delay in HSR hilly terrain.

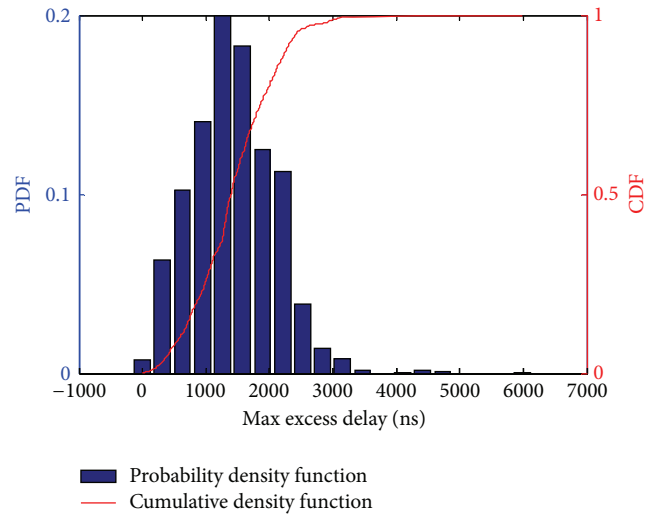

Figure 6: PDF and CDF of maximum excess delay values in HSR hilly terrain.

4. Doppler Frequency Shift

Doppler shift is used to describe the time selectivity of wireless channel, which is mainly due to relative motion between BS and train. In HSR scenario, the quick motion of train will cause large frequency shift and bring a serious ICI to wireless systems. Especially when the train is passing by the BS, the Doppler frequency changes from a positive value to a negative value in a very short period. So it is one crucial parameter of the HSR channel.

Theoretically, the Doppler frequency shift can be calculated by

$$f_d(t) = \frac{v}{\lambda}\cos(\theta(t)) = f_{\max}\cos(\theta(t)), \quad (6)$$

where v is the velocity of the HSR train in m/s, $\theta(t)$ is the angle of the incidence and λ is the wavelength. During our measurement campaign, the speed of the train is 295 kph, which is corresponding to the maximum Doppler frequency shift $f_{\max} = 656$ Hz.

With the assistance of SAGE algorithm, Doppler frequency shift of each MPC can be extracted as well as delay and amplitude. In the iterative estimation process of SAGE

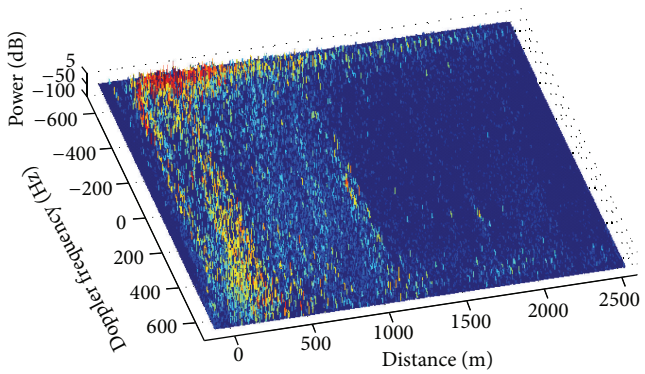

Figure 7: Doppler spectrums at different positions.

algorithm, the Doppler frequency shift resolution is set to 5 Hz.

Figure 7 shows the Doppler spectrums at different receiver positions. At each position, the Doppler shift and its corresponding power are plotted. The x-axis is the distance from the train to the intersection point, which equals 0 when the train passes the base station. And the y-axis is the frequency shift in Hz. In Figure 7 there is an abrupt change from $+f_{\max}$ to $-f_{\max}$ near the intersection point, which is corresponding to the Doppler shift of the LoS path. At the intersection point, this LoS Doppler frequency equals zero. At the same time, we can see different Doppler frequencies in Figure 7 besides the LoS path. This is different from the assumption that only LoS path exists in HSR environment [16]. Due to the rapid changing of the propagation environment and the randomness of the incidence angles, the Doppler frequencies of MPCs do not show strong continuity over the whole measured route. Most MPCs with different Doppler shifts do not last long and will disappear in a short time.

Abundant Doppler frequency bins can be found in AA and CA. This means the waves arrive at the train from different directions when the train is close to the BS. A specular frequency shift ray can be used to describe the LoS component. The Doppler feature of the reflected MPCs can be specified as random variable f_v, which follows a uniform distribution, that is, $f_v \sim U[f_{\max}, f_{\max}]$.

After the train passes the break point d_{BP2}, the hills near the railway block most of the rays from different directions and compose a "keyhole-" like environment near this break point. Only the MPCs travelling along the railway are able to pass through this "keyhole." Thereby, in DA and RA, very few Doppler shifts can be observed. There are only two dominant Doppler frequencies, that is, $-f_{\max}$ for LoS path and $+f_{\max}$ for the waves from the reflectors in front of the train along the railway.

5. TDL Channel Model

To provide a reference for future wireless system design, we need to build suitable models for the HSR hilly propagation environment. One simple and practical implementation is to model the channel impulse response with components at certain delays (taps). Hence the channel is modeled as a TDL filter [26]. Then the channel impulse response can be expressed by several taps with different delays and independent gains.

According to previous discussion in Section 3, it can be seen that the number of taps is correlated with the T-R distance. Four areas including AA, CA, DA, and RA are defined to partition the whole measured route.

Using the measured data, we parameterize the delay value and relative power of each tap in specific areas. All parameters are shown in Table 3. The delay and power of LoS path are set as 0 *ns* and 0 dBm, respectively. Together with path loss and fading models proposed in our previous work [19], it is possible to provide a fundamental model for evaluation of the radio interface and development of wireless communication system in HSR hilly scenario.

It should be mentioned that this TDL model with low complexity can be used only for calibration and comparison purposes. To support more accurate and complicated system

Table 3: TDL model for HSR hilly scenario.

Area	Tap index	Relative time delay (ns)	Average tap gain (dB)	Doppler shift
Adjacent area (AA)	1	0	0	$-f_{\max}$
	2	280	−8.7	f_v
	3	640	−17.5	f_v
	4	1350	−25.2	f_v
Close area (CA)	1	0	0	$-f_{\max}$
	2	200	−11.4	f_v
	3	450	−27.6	f_v
	4	520	−12.7	f_v
	5	860	−29	f_v
	6	1160	−28	f_v
	7	1230	−27.6	f_v
	8	1330	−23.8	f_v
	9	1390	−23.1	f_v
	10	1480	−25.9	f_v
	11	1590	−18.7	f_v
	12	1770	−29.1	f_v
	13	2100	−29.7	f_v
Distant area (DA)	1	0	0	$-f_{\max}$
	2	230	−9.2	$+f_{\max}$
	3	470	−15.3	$+f_{\max}$
	4	1140	−18.7	$+f_{\max}$
	5	1790	−22.4	$+f_{\max}$
Remote area (RA)	1	0	0	$-f_{\max}$
	2	410	−14.8	$+f_{\max}$
	3	2440	−18.3	$+f_{\max}$

Notes.
(1) f_v is a random variable and $f_v \sim U[-f_{\max}, +f_{\max}]$.
(2) The Doppler shift values are corresponding to the case when the train departs from the intersection point.

evaluations, more measurement campaigns need to be finished to build a geometric-based stochastic channel model for the HSR hilly scenario.

6. Conclusion

In this paper, we present the delay and Doppler frequency characteristics for HSR hilly scenario. It is shown that abundant reflected MPCs exist as well as the LoS component in this specific environment, especially when the train is close to the base station. The delay spread values would change with the transceiver distance, which can be divided into four areas, AA, CA, DA, and RA. The CDF of measured RMS delay spreads fits the log-normal distribution well. Although the rich-scattering environment provides more resolvable MPCs, the delay spread is not evidently improved, which may be due to the confined propagation space. The Doppler spectrum is also relevant to the train positions. An approximate estimation is suggested to describe the Doppler shifts of MPCs. Based on above analyses, a TDL model is proposed for the wideband HSR hilly channel which is expected to supply a reference for the design, evaluation, and improvement of the HSR wireless communication system.

Conflict of Interests

The authors declare that there is no conflict of interests regarding the publication of this paper.

Acknowledgment

This work has been partially supported by the National Natural Science Foundation of China (61201192), the National Basic Research Program of China (2012CB316002), the National S&T Major Project (2010ZX03006-002-03), the International S&T Cooperation Program (2012DFG12010), the Tsinghua University Initiative Scientific Research Program (2011Z02292), the Key Grant Project of Chinese Ministry of Education (313005), and the Open Research Fund of National Mobile Communications Research Laboratory, Southeast University.

References

[1] Wikipedia, "China Railway High-speed," 2013, http://en.wikipedia.org/wiki/China_Railway_High-speed.

[2] B. Ai, R. He, Z. Zhong et al., "Radio wave propagation scene partitioning for high-speed rails," *International Journal of Antennas and Propagation*, vol. 2012, Article ID 815232, 7 pages, 2012.

[3] T. Zhou, C. Tao, L. Liu, J. Qiu, and S. Rongchen, "High-speed railway channel measurements and characterizations: a review," *Journal of Modern Transportation*, vol. 20, no. 4, pp. 199–205, 2012.

[4] L. Liu, C. Tao, J. Qiu et al., "Position-based modeling for wireless channel on high-speed railway under a viaduct at 2.35 GHz," *IEEE Journal on Selected Areas in Communications*, vol. 30, no. 4, pp. 834–845, 2012.

[5] Y. Guo, J. Zhang, C. Tao et al., "Propagation characteristics of wideband high-speed railway channel in viaduct scenario at 2.35 GHz," *Journal of Modern Transportation*, vol. 20, no. 4, pp. 206–212, 2012.

[6] R. He, Z. Zhong, B. Ai, and J. Ding, "An empirical path loss model and fading analysis for high-speed railway viaduct scenarios," *IEEE Antennas and Wireless Propagation Letters*, vol. 10, pp. 808–812, 2011.

[7] R. He, Z. Zhong, B. Ai, G. Wang, J. Ding, and A. F. Molisch, "Measurements and analysis of propagation channels in high-speed railway viaducts," *IEEE Transactions on Wireless Communications*, vol. 12, no. 2, pp. 794–805, 2013.

[8] P. Aikio, R. Gruber, and P. Vainikainen, "Wideband radio channel measurements for train tunnels," in *Proceedings of the 48th IEEE Vehicular Technology Conference (VTC '98)*, pp. 460–464, May 1998.

[9] D. J. Cichon, T. Zwick, and W. Wiesbeck, "Ray optical modeling of wireless communications in high-speed railway tunnels," in *Proceedings of the IEEE 46th Vehicular Technology Conference (VTC '96)*, pp. 546–550, May 1996.

[10] M. Jia, "A modified method for predicting the radio propagation characteristics in tunnels," in *Proceedings of the 7th International Conference on Wireless Communications, Networking and Mobile Computing (WiCOM '11)*, IEEE, September 2011.

[11] A. Hrovat, G. Kandus, and T. Javornik, "A survey of radio propagation modeling for tunnels," *IEEE Communications Surveys & Tutorials*, 2013.

[12] R. He, Z. Zhong, B. Ai, J. Ding, Y. Yang, and A. Molisch, "Short-term fading behavior in high-speed railway cutting scenario: measurements, analysis, and statistical models," *IEEE Transaction on Antennas and Propagation*, vol. 61, no. 4, pp. 2209–2222, 2013.

[13] R. He, Z. Zhong, B. Ai, and J. Ding, "Propagation measurements and analysis for high-speed railway cutting scenario," *Electronics Letters*, vol. 47, no. 21, pp. 1167–1168, 2011.

[14] M. V. S. N. Prasad, K. Ratnamla, and P. K. Dalela, "Mobile communication measurements along railroads and model evaluations over Eastern-Indian rural regions," *IEEE Antennas and Propagation Magazine*, vol. 52, no. 5, pp. 131–141, 2010.

[15] WINNER2 WP1, "Radio channel measurement and analysis results," Deliverable D 1.1.2, ver 1.0. 30.9.2007, 2007.

[16] 3GPP, "TS 36.104 V9.3.0 3rd Generation Partnership Project; Technical Specification Group Radio Access Network; Evolved Universal Terrestrial Radio Access (eutra); Base Station (BS) radio transmission and reception (Release 9)," 2010.

[17] A. Mariscotti, A. Marrese, N. Pasquino, and R. Moriello, "Characterization of the propagation channel aboard trains," in *Proceedings of the 19th IMEKO TC-4 Symposium*, 2013.

[18] W. Dong, G. Liu, L. Yu, H. Ding, and J. Zhang, "Channel properties of indoor part for high-speed train based on wideband channel measurement," in *Proceedings of the 5th International ICST Conference on Communications and Networking in China (ChinaCom '10)*, pp. 1–4, August 2010.

[19] F. Luan, Y. Zhang, L. Xiao, C. Zhou, and S. Zhou, "Fading characteristics of wireless channel on high-speed railway in hilly terrain scenario," *International Journal of Antennas and Propagation*, vol. 2013, Article ID 378407, 9 pages, 2013.

[20] Y. Zhang, O. Edfors, P. Hammarberg et al., "A general coupling-based model framework for wideband MIMO Channels," *IEEE Transactions on Antennas and Propagation*, vol. 60, no. 2, pp. 574–586, 2012.

[21] C. Tao, L. Liu, J. Qiu, and Z. Tan, "Architecture and key techniques of broadband wireless access system for high speed

railway," *Telecommunications Science*, vol. 33, no. 5, pp. 95–101, 2010.

[22] B. H. Fleury, M. Tschudin, R. Heddergott, D. Dahlhaus, and K. I. Pedersen, "Channel parameter estimation in mobile radio environments using the SAGE algorithm," *IEEE Journal on Selected Areas in Communications*, vol. 17, no. 3, pp. 434–450, 1999.

[23] T. S. Rappaport, *Wireless Communications: Principles and Practice*, Prentice Hall, Upper Saddle River, NJ, USA, 1999.

[24] WINNER I WP5, "Final Report on Link Level and System Level Channel Models," D5.4, v.1.4, Algans, 2005.

[25] A. Algans, K. I. Pedersen, and P. E. Mogensen, "Experimental analysis of the joint statistical properties of azimuth spread, delay spread, and shadow fading," *IEEE Journal on Selected Areas in Communications*, vol. 20, no. 3, pp. 523–531, 2002.

[26] J. Sykora, "Tapped delay line model of linear randomly time-variant WSSUS channel," *Electronics Letters*, vol. 36, no. 19, pp. 1656–1657, 2000.